Numerical Heat Transfer, Part A, vol. 23, pp. 35–59, 1993

COMPARATIVE ANALYSIS OF THE FINITE-ELEMENT AND FINITE-DIFFERENCE METHODS FOR SIMULATION OF BUOYANCY-INDUCED FLOW AND HEAT TRANSFER IN CLOSED AND OPEN ENDED ANNULAR CAVITIES

K. Vafai and C. P. Desai
Department of Mechanical Engineering, Ohio State University, Columbus, Ohio 43210

The present work consists of comparative evaluation of the finite-element and finite-difference methods for the solution of complex fluid flow and heat transfer problems. The test case considered here is the problem of natural convection in an annular cavity. Both closed and open ended cases are considered. It was found that the finite-difference analysis succeeds in capturing minute details of the solution at high Rayleigh number flows and the finite-element method fails to do so. However, the finite-element method enjoys the advantage of providing sufficiently accurate results even with coarse meshes. This results in significant savings in computational costs without any sacrifice in the accuracy of the solution. Hence, the finite-element method can serve as an optimum tool for most problems of practical interest.

INTRODUCTION

Natural convection in annular cavities can be used to model processes in several domains of practical interest, such as nuclear reactors, thermal storage systems, and electric transmission cables. The main thrust in this area until about 1982 was directed toward simulation of the problem using a two-dimensional model [1–3]. This model gives fairly accurate results for cylinders that have a very high length to radius ratio, so that the analysis of the problem in the axial direction can be ignored. However, this turns out to be a poor assumption when the annulus has a finite length, because the flow retardation caused by the end walls has a direct influence on convection in the axial direction. For such cases, to capture the physics of the flow entirely, a full three-dimensional analysis of the problems becomes unavoidable.

Most of the three-dimensional numerical works have been performed for rectangular enclosures [4–9]. Only in the past decade have numerical studies been carried out for buoyancy-driven flow in a cylindrical annulus bounded by coaxial cylinders. Ozoe et al. [10] modified the vorticity vector potential approach for application in cylindrical polar coordinates to solve the natural convection problem for a vertical annulus heated from below. Later, Ozoe et al. [11] experimentally and numerically investigated the effects of inclination for the same problem. Takata et al. [12] performed a complete analytical and experimental investigation of natural convection in an inclined cylindrical annulus enclosed between heated inner and cooled outer cylinders. Three-dimensional governing equations, in terms of vorticity and vector potential, were transformed into finite-difference equations and solved numerically using the successive overrelaxation (SOR) procedure. They found that the three-dimensional structure of the fluid particles

A grant from the Ohio Supercomputer Center is acknowledged and appreciated.

1040-7782/93 $10.00 + .00

NOMENCLATURE

C_p	specific heat at constant pressure, J kg^{-1} K^{-1}
d	truncation error during time integration
g	acceleration due to gravity, m s^{-2}
k	thermal conductivity, W m^{-2} K^{-1}
L	length of the annular cavity, m
L_e	length of the extended computational domain, m
n	outward normal to a surface
Nu	Nusselt number
p	pressure, Pa
p^h	finite-element method approximation of pressure, Pa
Pr	Prandtl number ($= \nu/\alpha$)
q	heat flux vector
R_1	radius of the inner cylinder, m
R_2	radius of the outer cylinder, m
R_e	radius of the extended computational domain, m
Ra	Rayleigh number ($= g\beta R_2^3 \Delta T/\nu\alpha$)
t	time, s
T	temperature, K
T^h	finite-element method approximation for temperature, K
u_x	velocity in the x direction, m s^{-1}
u_y	velocity in the y direction, m s^{-1}
u_z	velocity in the z direction, m s^{-1}
u_x^h	finite-element method approximation for the x component of velocity, m s^{-1}
u_y^h	finite-element method approximation for the y component of velocity, m s^{-1}
u_z^h	finite-element method approximation for the z component of velocity, m s^{-1}
V	column vector consisting of all the unknown variables in the computational domain: u_x, u_y, u_z, p, T
x, y, z	Cartesian coordinates, m
α	thermal diffusivity, m^2 s^{-1}
β	coefficient of volume expansion, K^{-1}
ϵ	tolerance for truncation error in the transient analysis
μ	dynamic viscosity, kg m^{-1} s^{-1}
ν	kinematic viscosity, m^2 s^{-1}
ρ	density, kg m^{-3}

Subscripts

e	extended computational domain
x	x component
y	y component
z	z component
1	inner cylinder
2	outer cylinder
∞	condition at infinity

Superscripts

T	transpose of a matrix

was a coaxial double helix. This finding was confirmed by a flow visualization experiment conducted using suspended aluminum powder in glycerol. They also studied the effects of inclination angle on the flow field and heat transfer and found that the local Nusselt numbers show a fairly large dependence on the inclination angle. A three-dimensional numerical analysis for a short horizontal cylindrical annulus using a vorticity-velocity formulation was performed by Fusegi and Farouk [13]. Later, Rao et al. [14] used the Galerkin formulation of the finite-element method in a numerical study of three-dimensional natural convection in a horizontal porous annulus heated from the inner surface. They further clarified the spiral structure of the flow. A recent study on natural convectino in a horizontal annulus by Fukuda et al. [15] contains a direct numerical simulation (DNS), using an explicit leap-frog scheme, of turbulent natural convection in a horizontal annulus.

The results presented here have been obtained by using the finite-element method (FEM), which, while enjoying widespread use in structural problems, has a relatively short history in computational fluid mechanics. In recent years, however, both academic research and industrial practice have shown convincingly that FEM is a powerful tool in fluid mechanics. The great advantage of FEM over other methods is its inherent flexibility in treating arbitrarily complex flow domains and boundary conditions. Unstructured

grids can be designed that allow areas of interest to be studied in great detail without need for excessive grid points throughout the entire flow domain. FEM allows the natural and correct imposition of boundary conditions on curved boundaries, which is a very important consideration in the present study. In addition, FEM has an elegant mathematical formulation that allows derivation of comprehensive error estimates and determination of solutions accurate to within user-prescribed tolerances. At the same time, fluid simulation with FEM allows access to the wealth of preprocessing and postprocessing packages of powerful graphics available in the structural engineering field.

Despite the fact that the FEM is becoming a popular numerical tool in the solution of fluid mechanics and heat transfer problems, researchers have not yet been able to predict with certainty whether the FEM or the finite-difference method is more advantageous in different flow situations. Limited material is available in the literature pertaining to the comparison between these two methods for problems of complex, three-dimensional fluid dynamics. Some comparisons have been carried out in the past using pure conduction problems as test cases. As far as problems of convection heat transfer are concerned, one study of significance was carried out by de Vahl Davis and Jones [16], who used the well-studied problem of natural convection in a square cavity to compare several numerical techniques for fluid dynamics and heat transfer problems. Within the range of Rayleigh numbers considered, they found that the FEM gave the best results. However, some finite-difference solutions also gave solutions of comparable accuracy. There is a definite need for more comparative analysis of these two methods, especially for complex flow and heat transfer problems. Later, Ozoe et al. [17] made a numerical study of natural convection in confined rectangular regimes by using an FEM based on a second-order approximation. In their study, the average Nusselt number was extrapolated to zero-element size. They found that a second-order approximation for the unknown functions produces much better results than the linear approximation, but the discretization error can never be neglected. They concluded that computations for several element sizes for the same conditions, followed by extrapolation to zero element size, are essential to obtain accurate results.

The present study provides such a comparative evaluation of the finite-difference and finite-element methods for the solution of some complicated fluid flow and heat transfer problems. The test cases for this study are the transient, three-dimensional process of buoyancy-induced flow and heat transfer in both closed and open ended annular cavities. The numerical procedure used in this work is based on the Galerkin weighted residual method of finite-element formulation. FEMs are considered to be more efficient than finite-difference methods (FDMs) in providing solutions of first-order accuracy, but the latter are more efficient if the fine structure of the fluid motion is required. This work provides a quantitative and qualitative confirmation of these observations for natural convection.

FORMULATION

Assumptions

The annulus is assumed to be placed horizontally, and gravity is confined to the negative x direction. The temperature and flow fields are found to be symmetrical with

respect to the vertical plane, and as a result the region of interest is only half the annulus. It is assumed in the analysis that the thermophysical properties of the walls and the fluid are independent of temperature except for the density in the buoyancy term, that is, the Boussinesq approximation is invoked. The fluid is assumed to be Newtonian and incompressible. Viscous heat dissipation in the fluid is assumed to be negligible in comparison to conduction and convection. The fluid motion and heat transfer in the cavity are assumed to be laminar.

Model Equations

The problem is modeled for transient natural convection in an incompressible fluid. The Boussinesq approximation is used for the density in the gravitational body force term, where its variation causes the buoyancy force necessary to drive the flow. The equations governing this process in Cartesian coordinates are written in nondimensional form as

Continuity

$$\frac{\partial u_x}{\partial x} + \frac{\partial u_y}{\partial y} + \frac{\partial u_z}{\partial z} = 0 \tag{1}$$

x momentum

$$\left(\frac{\mathrm{Ra}}{\mathrm{Pr}}\right)^{1/2}\left\{\frac{\partial u_x}{\partial t} + u_x\frac{\partial u_x}{\partial x} + u_y\frac{\partial u_x}{\partial y} + u_z\frac{\partial u_x}{\partial z}\right\} = -\frac{\partial p}{\partial x} + \left(\frac{\mathrm{Ra}}{\mathrm{Pr}}\right)^{1/2} T + \frac{\partial^2 u_x}{\partial x^2} + \frac{\partial^2 u_x}{\partial y^2} + \frac{\partial^2 u_x}{\partial z^2} \tag{2}$$

y momentum

$$\left(\frac{\mathrm{Ra}}{\mathrm{Pr}}\right)^{1/2}\left\{\frac{\partial u_y}{\partial t} + u_x\frac{\partial u_y}{\partial x} + u_y\frac{\partial u_y}{\partial y} + u_z\frac{\partial u_y}{\partial z}\right\} = -\frac{\partial p}{\partial y} + \frac{\partial^2 u_y}{\partial x^2} + \frac{\partial^2 u_y}{\partial y^2} + \frac{\partial^2 u_y}{\partial z^2} \tag{3}$$

z momentum

$$\left(\frac{\mathrm{Ra}}{\mathrm{Pr}}\right)^{1/2}\left\{\frac{\partial u_z}{\partial t} + u_x\frac{\partial u_z}{\partial x} + u_y\frac{\partial u_z}{\partial y} + u_z\frac{\partial u_z}{\partial z}\right\} = -\frac{\partial p}{\partial z} + \frac{\partial^2 u_z}{\partial x^2} + \frac{\partial^2 u_z}{\partial y^2} + \frac{\partial^2 u_z}{\partial z^2} \tag{4}$$

Energy

$$\left(\frac{\mathrm{Ra}}{\mathrm{Pr}}\right)^{1/2}\left\{\frac{\partial T}{\partial t} + u_x\frac{\partial T}{\partial x} + u_y\frac{\partial T}{\partial y} + u_z\frac{\partial T}{\partial z}\right\} = \frac{\partial^2 T}{\partial x^2} + \frac{\partial^2 T}{\partial y^2} + \frac{\partial^2 T}{\partial z^2} \tag{5}$$

For the two-dimensional case, which is also studied here, all the variations in the z direction are ignored.

Equations (1)–(5) were cast in nondimensional form by using the following nondimensional variables:

$$x^* = \frac{x}{R_2} \qquad y^* = \frac{y}{R_2} \qquad z^* = \frac{z}{R_2}$$

$$u_x^* = \frac{u_x R_2}{\alpha(\mathrm{Ra\ Pr})^{1/2}} \qquad u_y^* = \frac{u_y R_2}{\alpha(\mathrm{Ra\ Pr})^{1/2}} \qquad u_z^* = \frac{u_z R_2}{\alpha(\mathrm{Ra\ Pr})^{1/2}}$$

$$T^* = \frac{T - T_\infty}{T_1 - T_\infty} \qquad p^* = \frac{pR_2^2}{\mu\alpha(\mathrm{Ra\ Pr})^{1/2}} \qquad t^* = \frac{t\alpha(\mathrm{Ra\ Pr})^{1/2}}{R_2^2}$$

The subscripts are dropped for convenience.

These five equations in terms of five unknowns, along with the appropriate initial and boundary conditions, fully describe the transient, convective energy transfer process in an annulus.

Initial Conditions

As mentioned above, all the walls of the annulus are assumed to be initially at uniform, ambient temperature, and the fluid is assumed to be stagnant and at ambient temperature throughout the computational domain. This condition is stated mathematically as

$$u_x = u_y = u_z = T = 0 \qquad \text{at } t = 0 \tag{6}$$

Boundary Conditions

Since three different models are considered here, the boundary conditions for each case are explained along with the results for the respective cases.

NUMERICAL SCHEME

A Galerkin-based FEM was employed to solve the system of differential equations described in the previous section. The application of this technique is well described by Taylor and Hood [18] and Gresho et al. [19], and its application in the finite-element code used in the present work is also well documented [20]. This scheme is briefly explained here.

The continuum domain is first divided into a set of simply shaped, nonoverlapping regions called elements, within each of which the unknown variables u_x, u_y, u_z, p, and T are approximated by using the following equations:

$$u_x \approx u_x^h = \phi^T[U_x] \tag{7a}$$

$$u_y \approx u_y^h = \phi^T[U_y] \tag{7b}$$

$$u_z \approx u_z^h = \phi^T[U_z] \tag{7c}$$

$$p \approx p^h = \Psi^T[P] \tag{7d}$$

$$T \approx T^h = \theta^T[T] \tag{7e}$$

where ϕ, Ψ, and θ are the interpolation functions for velocity, pressure, and temperature, respectively. These are local functions of the nodal coordinates for that element as well as the independent variables. The vectors $[U_x]$, $[U_y]$, $[U_z]$, $[P]$, and $[T]$ consist of the values of the respective variables at the nodes of the element.

Substituting these basis functions into the governing equations and boundary conditions yields a residual (error) in each of the equations, which can be stated as follows:

Continuity

$$f_1(\phi, U_x, U_y, U_z) = E_1 \tag{8a}$$

Momentum

$$f_2(\phi, \Psi, \theta, U_x, U_y, U_z, P, T) = E_2 \tag{8b}$$

Energy

$$f_3(\phi, \theta, U_x, U_y, U_z, T) = E_3 \tag{8c}$$

where E_1, E_2, and E_3 are the residuals (errors) resulting from use of the finite-element approximations.

The Galerkin form of the method of weighted residuals seeks to reduce these errors to zero in a weighted sense, that is, by making the residuals orthogonal to the interpolation functions of each element. These orthogonality conditions are expressed by

$$\int_V \Psi E_1 \, dV = \int_V \Psi f_1 \, dV = 0 \tag{9a}$$

$$\int_V \phi E_2 \, dV = \int_V \phi f_2 \, dV = 0 \tag{9b}$$

$$\int_V \theta E_3 \, dV = \int_V \theta f_3 \, dV = 0 \tag{9c}$$

This procedure yields a system of equations for each element, which can be written as

$$\bar{M} \frac{\partial V}{\partial t} + \bar{K}(V)V = \bar{F} \tag{10}$$

where V is a column vector of the unknown variables, F is a force vector (incorporating the boundary conditions), M is a mass matrix, and K is a stiffness matrix (representing the diffusion and convection of energy).

Equation (10) represents the discrete analog of the governing continuum equations, Eqs. (1)–(5), for an individual fluid element. The discrete representation of the entire

continuum region of interest is obtained through an assemblage of elements such that interelement continuity of velocity and temperature is enforced. The result of such an assembly process is a system of matrix equations of the form given by Eq. (10).

To obtain a transient solution, the continuous time derivative needs to be replaced by an approximation for the history of the time-dependent variable over a small portion of the problem time scale. In other words, some sort of a time-dependent integration scheme is necessary. The result is an incremental procedure that advances the solution in discrete steps of time. The trapezoidal scheme developed by Gresho et al. [19] was used for the time discretization of the governing equations. By an appropriate combination of two common, second-order-accurate integration techniques, the implicit trapezoidal rule (TR) and an explicit Adams-Bashforth (AB) formula, they developed a stable time integration scheme in which the size of the time step can be economically and automatically varied. This was accomplished solely on the basis of temporal accuracy requirements, by obtaining a good estimate of the local (single step) time truncation error. This also provides us with insight into the prevailing "physics" of the flow by monitoring the variable time scale. The algorithm automatically selects the appropriate time step size, thus providing a cost-effective method, in that the step size is increased whenever possible and decreased only when necessary.

Since an implicit time integrator has been used in the present case for discretization of the governing equations in time, at each time step a nonlinear system of equations needs to be solved. Gresho et al. [19] showed that with the predictor-corrector scheme used in the present code, if the error tolerance of the user-specified local time truncation is set to 0.001–0.005 or 0.1–0.5% error, then the predictor is sufficiently accurate that only one Newton-Raphson iteration is required at each time step to achieve convergence. This, however, can be very expensive in studies like the present one, in which even one iteration can take a considerable amount of CPU time when the Newton-Raphson method is used. To reduce this time, we have used the quasi-Newton solution algorithm to solve the nonlinear system at each time step. This algorithm can be shown to be superlinearly convergent, and in practice its convergence rate approaches that of the Newton-Raphson method, while the time for one iteration of the quasi-Newton algorithm is typically 10–20% of the time for a Newton-Raphson iteration. A complete description of this quasi-Newton method in the FEM simulation of incompressible fluid flows is given by Engelman et al. [21].

The advantage of the quasi-Newton method in the framework of the transient algorithm is that the reformation of the Jacobian matrix need only be performed every N time steps. Of course, a balance must be found between the number of steps N and the quasi-Newton iterations required at each time step to achieve convergence. Typically, if $N = 2$ or 3, a savings can be attained in computer time of the order of 50% over the one-step Newton-Raphson method.

HEAT TRANSFER CALCULATIONS

The Nusselt number associated with the convective flow in this case is defined by

$$\mathrm{Nu} = q_n = \frac{\partial T}{\partial n} \tag{11}$$

where n denotes the outward pointing normal from the surface over which the heat flux is to be calculated. This definition of the Nusselt number is used to represent all the heat transfer results in the present study.

RESULTS AND DISCUSSION

In this work, a comparative study of finite-difference and finite-element solutions for the problem of natural convection in annular cavities has been presented. The finite-element solutions obtained using FIDAP are compared with finite-difference solutions reported in the literature by previous investigators [1, 12, 22, 23]. The numerical procedure outlined in the previous section forms the basis of this general purpose, finite-element code for solving problems of incompressible fluid flow. The inherent advantages and disadvantages of using one technique over the other for particular flow situations are also explained in this study. Detailed results for the flow and temperature fields are presented in each case to emphasize the accuracy of our comparisons.

The following three geometries, which fall under the general category of annular cavities, were considered as fundamental cases for the present study:

1. Two-dimensional annulus.
2. Three-dimensional closed annulus.
3. Three-dimensional open annulus.

All the results presented here are for a hot inner cylinder ($T_1 = 1$) and cold outer cylinder ($T_2 = 0$). Analysis of buoyancy-driven flows caused by the temperature difference between the hot inner and cold outer cylinder for case 1 have been carried out by researchers in the past, while cases 2 and 3 have been analyzed recently. These results provide reliable information for comparing the two solution methods. Results showing in detail a quantitative and qualitative comparison of the flow and temperature fields are presented here. Also, the Nusselt number has been used as a basis for comparison wherever possible.

Case 1: Comparison of Results for Two-Dimensional Annuli

The two-dimensional model for the study of buoyancy-driven flow in an annulus is shown in Fig. 1. The boundary conditions for this problem are as follows:

Surface (1) of the inner cylinder

$$u_x = u_y = 0 \qquad T = T_1 \qquad \text{at } r = \frac{R_1}{R_2} \qquad 0 \le \phi \le 180 \tag{12}$$

Surface (2) of the outer cylinder

$$u_x = u_y = 0 \qquad T = T_2 \qquad \text{at } r = 1 \qquad 0 \le \phi \le 180 \tag{13}$$

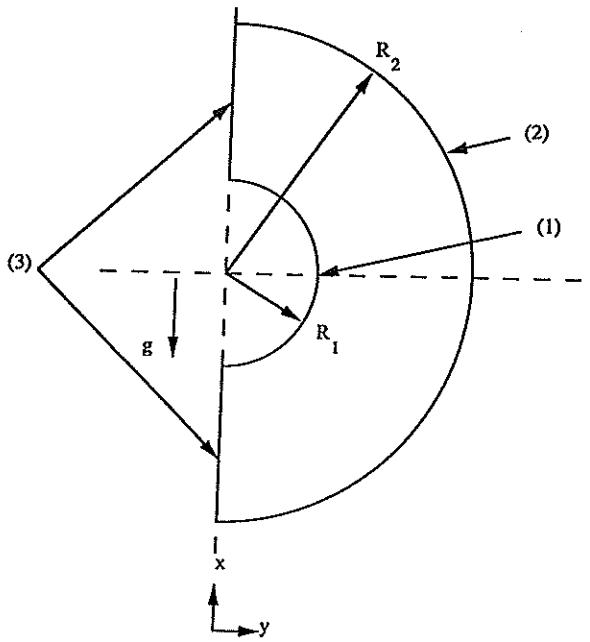

Fig. 1 Physical model and computational domain for the two-dimensional study.

Symmetry plane (3)

$$u_y = 0 \qquad \frac{\partial u_x}{\partial y} = \frac{\partial T}{\partial y} = 0 \qquad \text{at } \phi = 0 \qquad \phi = 180 \qquad \frac{R_1}{R_2} \le r \le 1 \tag{14}$$

Results obtained by Kuehn and Goldstein [1] for a two-dimensional annulus were used for benchmarking our results in this case. As mentioned above, their work consisted of an experimental investigation as well as a steady state, two-dimensional, finite-difference numerical simulation of natural convection in a horizontal concentric annulus. A vorticity-streamfunction approach was used by these authors to transform the governing equations. The computations were carried out for an annulus with a radii ratio of 2.6 with air (Pr = 0.7) and water (Pr = 5) as working fluids. The basic grid consisted of 304 nodes (16 in the radial direction and 19 in the angular direction) and had to be increased to 416 nodes (16 × 26) for higher Rayleigh numbers. To compare the results obtained by the present method with those obtained by Kuehn and Goldstein, an annulus with the same dimensions and with the same working fluid was considered. Nine-node quadrilateral elements were used for our study. The mesh consisted of 187 grid points (11 points in the radial direction and 17 points in the angular direction) for the low Rayleigh number cases and had to be increased to 357 point (17 × 21) for the cases with higher Rayleigh numbers. A typical run took 20–30 s to give converged steady state solutions. Streamlines and isotherms that we obtained are presented along with the results of Kuehn and Goldstein [1] in Fig. 2. The Rayleigh numbers and Prandtl num-

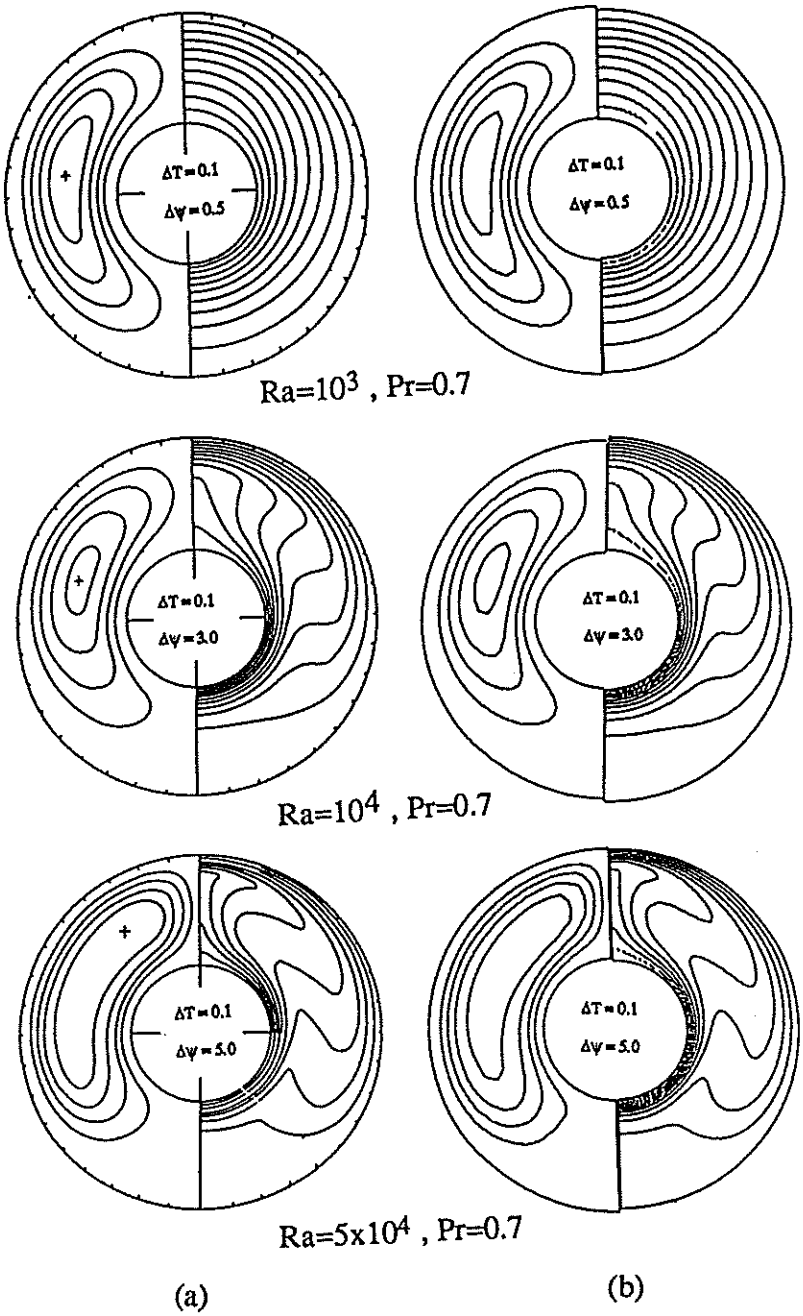

Fig. 2 Comparison of streamlines and isotherms for two-dimensional annuli: (*a*) Kuehn and Goldstein [1] and (*b*) present work. ([Figure 2*a* is reprinted with permission from Cambridge University Press.]

bers associated with each of these cases are given in the figure. Comparison of the results clearly illustrates that the two methods give exactly the same solution. Even the magnitudes of the streamlines match perfectly. The exact agreement between the results can also be seen by comparing the centers of rotation of the recirculating vortex obtained by the two methods. These centers are located at exactly the same position. Furthermore, a comparison of the mean Nusselt numbers obtained at the inner and outer cylinders showed agreement within 1%.

Case 2: Comparison of Results for Three-Dimensional Closed Annuli

Referring to Fig. 3, the boundary conditions applied for this problem are as follows:

Surface (1) of the inner cylinder

$$u_x = u_y = u_z = 0 \qquad T = T_1 \qquad \text{at } r = \frac{R_1}{R_2} \qquad 0 \le z \le \frac{L}{R_2} \tag{15}$$

Surface (2) of the outer cylinder

$$u_x = u_y = u_z = 0 \qquad T = T_2 \qquad \text{at } r = 1 \qquad 0 \le z \le \frac{L}{R_2} \tag{16}$$

Symmetry plane (3)

$$u_y = 0 \qquad \frac{\partial u_x}{\partial y} = \frac{\partial u_z}{\partial y} = \frac{\partial T}{\partial y} = 0 \tag{17}$$

Closed end walls (4) of the annulus

$$u_x = u_y = u_z = 0 \qquad \frac{\partial T}{\partial z} = 0 \qquad \text{at } z = 0 \text{ and } z = L \tag{18}$$

An in-depth study of the three-dimensional buoyancy-induced flow in an annulus bounded by horizontal, coaxial cylinders with closed ends was carried out by Vafai and Ettefagh [22]. They performed a numerical simulation using a vorticity-vector potential approach for an annulus with a radii ratio of $R_2/R_1 = 2.6$ and length to outer cylinder radius ratio of $L/R_2 = 4$. Calculations were performed for Rayleigh numbers of 4.3×10^3 and 4.3×10^4 using air (Pr = 0.7) as the working fluid. They presented results for the flow and temperature fields in radial planes at different axial locations throughout the annulus length. The viscous shearing effect of the end wall adds three-dimensional complexity to the flow and temperature fields in the region close to the end wall. This effect of the end wall thoroughly investigated by Vafai and Ettefagh [22].

In the work of Vafai and Ettefagh [22] the transient three-dimensional governing equations were formulated in terms of vorticity and vector potential. Their parabolic equations were solved by the modified form of the three-dimensional alternating-direction implicit (ADI) method developed by Brian [24], and at each time step the

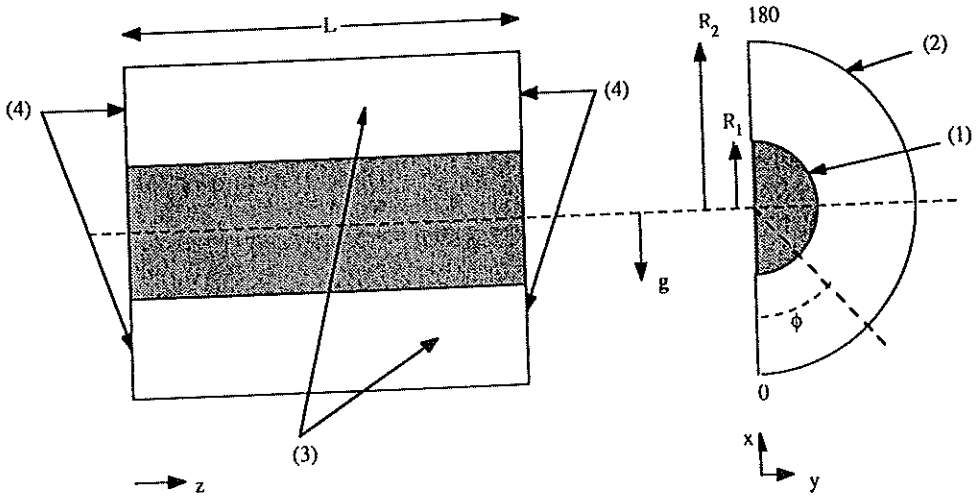

Fig. 3 Physical model and computational domain used for the three-dimensional closed annulus.

elliptic equations were solved by the three-dimensional extrapolated Jacobi scheme. Various combinations of mesh sizes and time increments were tried to select one that produces grid and time increment independent results.

For the Rayleigh number of 4.3×10^3, the isotherms are slightly eccentric circles (not shown here), indicating the presence of a very weak convective flow. The end wall effects in this case are negligible, and the core region in which the flow field is essentially two-dimensional extends almost the entire length of the cylinder. The axial component of velocity exists in regions close to the end wall, indicating the presence of a three-dimensional flow field. The magnitude of the axial velocities is very low, however, compared to the velocity vectors in the radial plane. Our study made use of 2805 grid points ($15 \times 17 \times 11$), while Vafai and Ettefagh [22] used 9975 grid points ($25 \times 19 \times 21$). The finite-element code required approximately 20 min while the finite-difference code developed by Vafai and Ettefagh required 30 min of CPU time on the Cray-YMP supercomputer. A comparison of the velocity magnitudes obtained from the two studies is given in Table 1. Since the nondimensionalization used in the two studies is different, the conversion was made by using the factor $\sqrt{\text{Ra Pr}}$. Also, contours of the axial component of velocity in two planes located very close to the end walls are shown in Fig. 4. In the results presented by Vafai and Ettefagh [22], the dotted lines

Table 1 Comparison of Flow Field Results for $\text{Ra} = 4.3 \times 10^3$ (Closed Annulus)

	Maximum value of the velocity vector in the radial plane		
Axial position	FDM	FEM	Difference, %
L/40	8.56	8.71	1.70
L/8	12.75	12.81	1.25
L/2	13.17	13.31	0.90

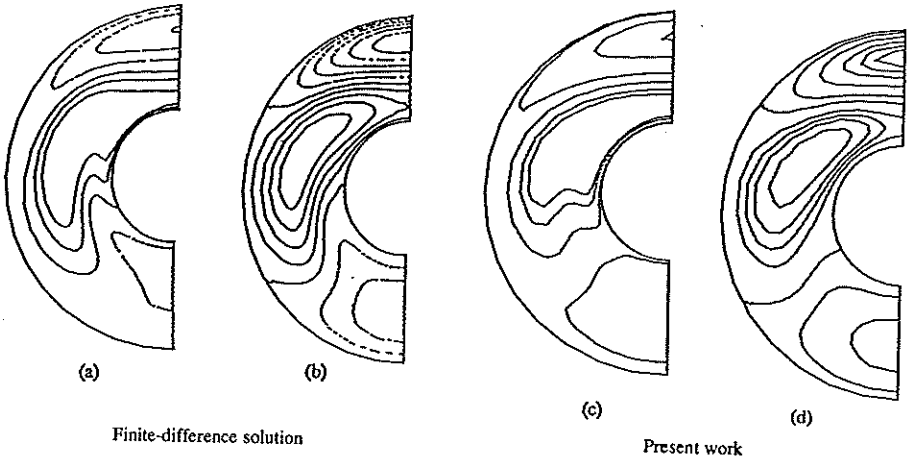

Fig. 4 Comparison of axial velocity contours for the closed annulus ($Ra = 4.3 \times 10^3$) at different locations: (*a* and *c*) $z = L/40$ and (*b* and *d*) $z = L/8$. [Figure 4*a* and 4*b* are reprinted with permission from *International Journal of Heat and Mass Transfer*, vol. 34: K. Vafai and J. Ettefagh, An Investigation of Transient Three-Dimensional Natural Convection in a Horizontal Annulus, copyright © 1991, Pergamon Press Ltd.]

depict the negative axial velocities and solid contours depict the positive axial velocities of the fluid. The opposite is used in the present study. From the values given and from the figure, it can be seen that results of the two studies are in quite good agreement. The slight qualitative discrepancy in the axial velocity contours is attributed to the inherent differences between the FDM and FEM used for the solutions of the problem.

The mean Nusselt numbers over the inner and outer cylinder surfaces at the top angular plane ($\phi = 180$) were also calculated for the two solutions. The angle ϕ is measured from the lowermost point of the annulus, as shown in Fig. 3. These measurements are given in Table 2. From the values shown, we see that our results fall within 2% of the finite-difference results.

For a higher Rayleigh number ($Ra = 4.3 \times 10^4$), as used in the study by Vafai and Ettefagh [22], the effect of the end wall penetrates farther into the annulus, and the complicated three-dimensional nature of the flow persists over a larger portion of the computational domain. In other words, the length of the core region in which the two-dimensional nature of the flow field persists becomes smaller [22]. Figure 5 shows the isotherms at the mid-axial plane and at the end wall of the annulus as predicted by Vafai and Ettefagh [22] and as obtained here using the finite-element algorithm. Comparison of these isotherms shows good agreement between the two results. The clustering of isotherms around the inner and outer cylinders at the mid-axial plane is a result of the higher strength of the recirculating flow in that region. The retardation caused by the end

Table 2 Comparison of Mean Nusselt Numbers at the Top Angular Plane ($Ra = 4.3 \times 10^3$)

Inner cylinder			Outer cylinder		
FDM	FEM	Difference, %	FDM	FEM	Difference, %
0.70	0.715	1.71	1.3	1.316	1.07

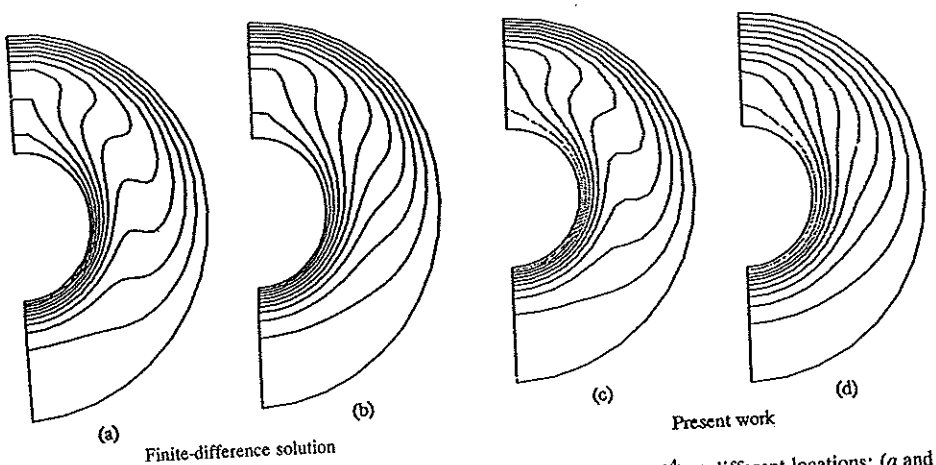

Fig. 5 Comparison of isotherms for the closed annulus ($Ra = 4.3 \times 10^4$) at different locations: (*a* and *c*) mid-axial plane and (*b* and *d*) end well. [Figure 5*a* and 5*b* are reprinted with permission from *International Journal of Heat and Mass Transfer*, vol. 34: K. Vafai and J. Ettefagh, An Investigation of Transient Three-Dimensional Natural Convection in a Horizontal Annulus, copyright © 1991, Pergamon Press Ltd.]

wall causes a reduction in velocities and hence the clustering of the isotherms at the inner and outer cylinders diminishes.

To further evaluate the accuracy of our results, a Nusselt number comparison was made. Figure 6*a* shows a three-dimensional "fishnet" plot of the outer cylinder Nusselt number as a function of the angular and axial locations (reproduced from Vafai and Ettefagh [22]). Due to the plotting limitations of the finite-element code, a similar plot for our results could not be obtained. Hence, the Nusselt number values at $\phi = 180$ for the outer cylinder have been plotted as a function of axial position in Fig. 6*b*. This location was chosen because the maximum variations in the Nusselt number exist at this position. Although the Nusselt number values lie in the same range for the results obtained from the two approaches, the variations of the Nusselt number, especially at regions close to the end wall, are found to be different. The present study failed to capture the fluctuations of the Nusselt number at regions close to the wall. Only one maximum was observed (Fig. 6*b*). To verify the suspicion that this result was due to an insufficient number of elements close to the walls, an intensive mesh size study was carried out. Since the axial mesh size is the critical parameter in this case, we concentrated on the effect of axial grid size. The number of grid points in the axial direction was varied from 17 for the initial runs to up to 61 to study its influence on the solution. Results obtained for three of the mesh sizes considered are shown in Fig. 6*b*. From these plots, it is observed that the solution remains almost unchanged when the number of points is varied from 31 to 41 in the axial direction. Further increasing the number of grid points in the axial direction did not affect the solution at all, showing that the results obtained were independent of mesh size.

The radial and angular mesh sizes were also varied to determine their influence on the solution. It was observed that no amount of mesh refinement in any of the three directions captures the sharp fluctuations in the Nusselt number at regions close to the end wall. Once again, velocity fields are compared for the two cases, quantitatively by considering the magnitudes of the velocity vectors, and qualitatively by using the con-

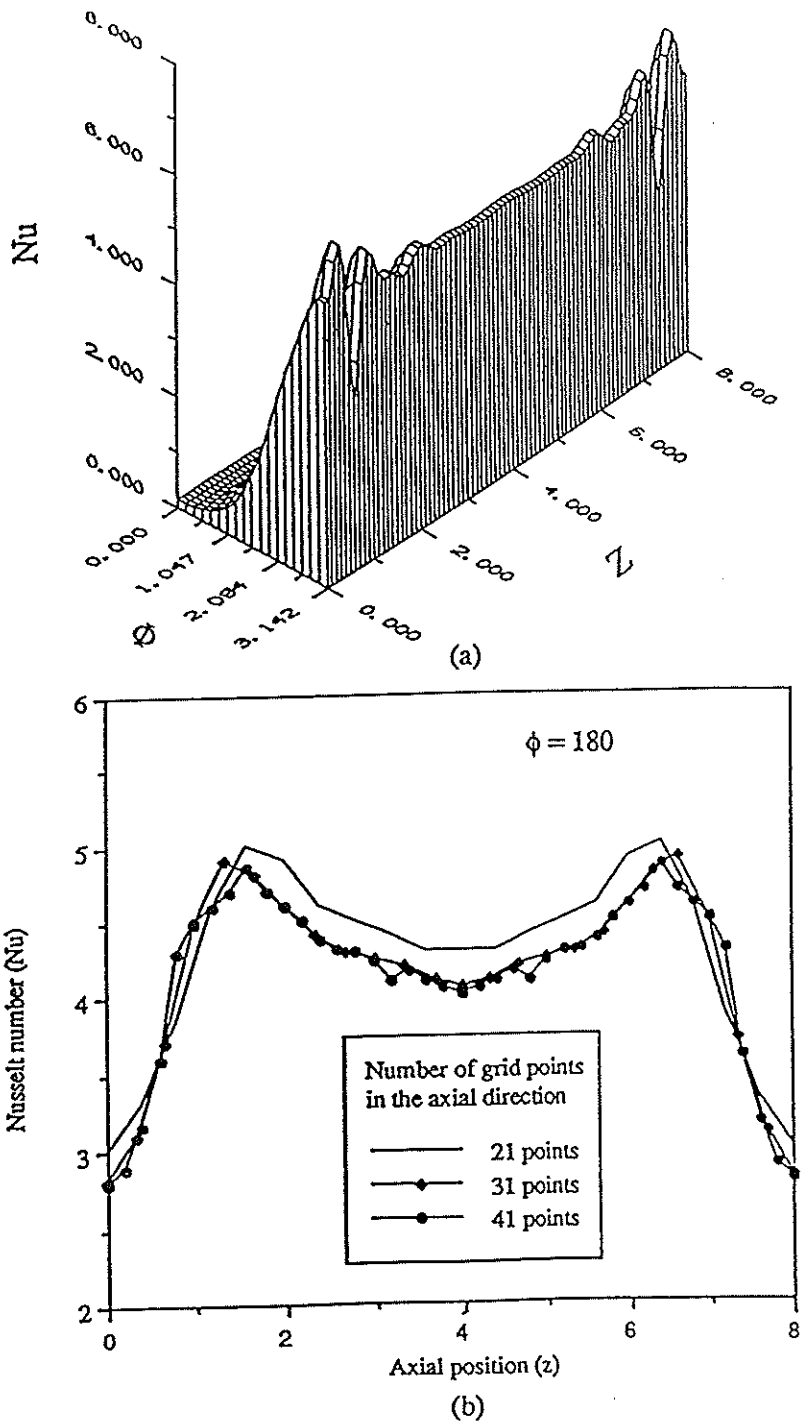

Fig 6 Comparison of the outer cylinder Nusselt number for the closed annulus ($Ra = 4.3 \times 10^4$): (*a*) finite-difference solution and (*b*) present work. [Figure 6*a* is reprinted with permission from *International Journal of Heat and Mass Transfer*, vol. 34: K. Vafai and J. Ettefagh, An Investigation of Transient Three-Dimensional Natural Convection in a Horizontal Annulus, copyright © 1991, Pergamon Press Ltd.]

Table 3 Comparison of Flow Field Results for $Ra = 4.3 \times 10^4$ (Closed Annulus)

	Maximum value of velocity in the radial plane			
		FEM		
Axial position	FDM	$K = 21$	$K = 31$	$K = 41$
$L/40$	59.9	65.1	62.4	61.9
$3L/80$	64.0	69.9	65.6	65.2
$3L/40$	76.0	75.2	73.2	72.8
$L/10$	78.0	73.9	72.0	71.9
$17L/80$	79.0	84	82.1	81.7
$L/2$	78.5	79.9	78.9	78.2

tour plots of the axial component of the velocity. Results for the same meshes are presented here (Table 3) to show the effect of mesh size on the solution. Comparison of the axial velocity contours is shown in Fig. 7, where the discrepancy in the contours obtained from the two techniques is obvious. From Table 3, it can be seen that as the mesh size is decreased, the magnitudes of the velocity vectors decrease, verifying the fact that as the mesh is refined, the discretized domain becomes stiffer, giving lower values for the variables. The difference in the flow fields at regions close to the end wall manifests itself into a completely different temperature field and Nusselt number distribution at these locations. The maximum difference in the magnitudes of the velocities was found to be 7.82% at the location $L/10$ from the end wall.

The above results clarify some of the inherent advantages and disadvantages of the FEM over the FDM for this class of problems. For low Rayleigh numbers, the solutions obtained using the FEM are sufficiently accurate to predict the flow and temperature fields. The magnitude and variation of the local Nusselt number over the surfaces of the annular geometry are also predicted accurately by the FEM. These solutions can be obtained by using a mesh that is very coarse compared to that used in the finite-

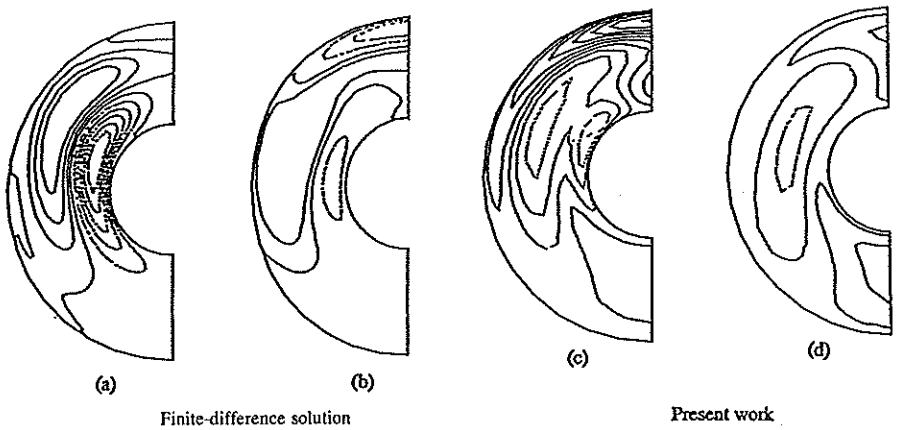

Fig. 7 Comparison of axial velocities for a closed annulus at different locations ($Ra = 4.3 \times 10^4$, $Pr = 0.7$): (*a* and *c*) $z = L/40$ and (*b* and *d*) $z = L/10$. [Figure 7*a* and *b* are reprinted with permission from *International Journal of Heat and Mass Transfer*, vol. 34: K. Vafai and J. Ettefagh, An Investigation of Transient Three-Dimensional Natural Convection in a Horizontal Annulus, copyright © 1991, Pergamon Press Ltd.]

difference technique, and this results in significant savings in computational costs. However, at higher Rayleigh numbers, where greater resolution in necessary to capture the intricacies of the flow and temperature fields, the accuracy of the solution deteriorates. The sharp variations in the flow and temperature fields cannot be captured by the FEM, irrespective of the extent of mesh refinement. Thus, in spite of the fact that a significant amount of CPU time can be saved, some loss of accuracy results at higher Rayleigh numbers. However, the results, especially the Nusselt number values, fall within a reasonable range that might be acceptable in most cases of practical interest. Hence, for a wide variety of engineering design problems, where results within relatively relaxed tolerances can be acceptable but computational costs are a serious consideration, the FEM serves as a good solution technique.

Results obtained by Takata et al. [12] were also used to compare the solutions for the three-dimensional closed annulus. Numerical results obtained by these investigators along with the experimental verification provide a strong basis for verifying the validity of the numerical code used in the present study. Takata et al. formulated the problem in a vorticity-vector potential form, and the equations so obtained were discretized by using a FDM. The numerical computations were performed for an annulus with a radii ratio of $R_2/R_1 = 2$, length to outer cylinder radius ratio $L/R_2 = 2$, $\mathrm{Ra} = 10^5$, and $\mathrm{Pr} = 5000$.

Only one Prandtl number was used, and the investigators concentrated only on the steady state solution of the problem. It appears that the high Prandtl number fluid was necessary in their case to obtain stability of the numerical scheme used. Figure 8 shows isotherms at the mid-axial plane and at the end wall of the annulus at steady state. It can be seen that the results obtained using the FEM (present work) are in very good agreement with the results of Takata et al. [12]. To further verify the accuracy of our solution, the local Nusselt numbers for the outer cylinder were compared at three different angular positions (Fig. 9). Once again, our results show good agreement with those of Takata et al. [12]. However, again there are some qualitative differences. The maximum differ-

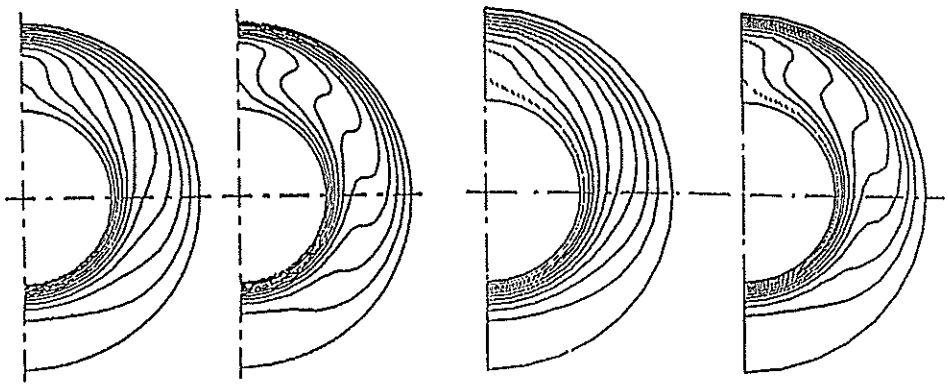

Fig. 8 Comparison of isotherms for the closed annulus at different locations ($\mathrm{Ra} = 10^5$, $\mathrm{Pr} = 5 \times 10^3$): (*a*) end wall, Takata et al. [12], (*b*) mid-axial plane. Takata et al. [12], (*c*) end wall, present work, and (*d*) mid-axial plane, present work. [Figure 8*a* and 8*b* are reprinted with permission from *International Journal of Heat and Mass Transfer*, vol. 27: Y. Takata, K. Iwashige, K. Fukuda, and S. Hasegawa, Three-Dimensional Natural Convection in an Inclined Cylindrical Annulus, copyright © 1984, Pergamon Press Ltd.]

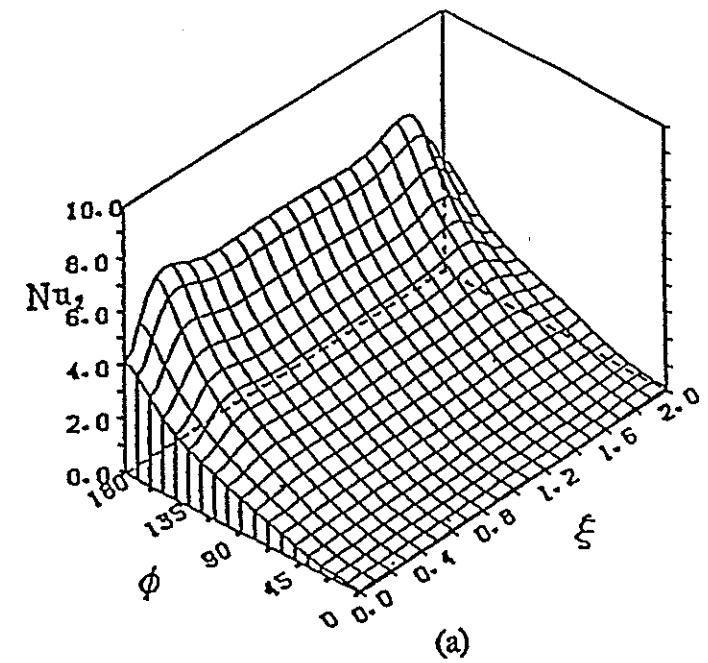

(a)

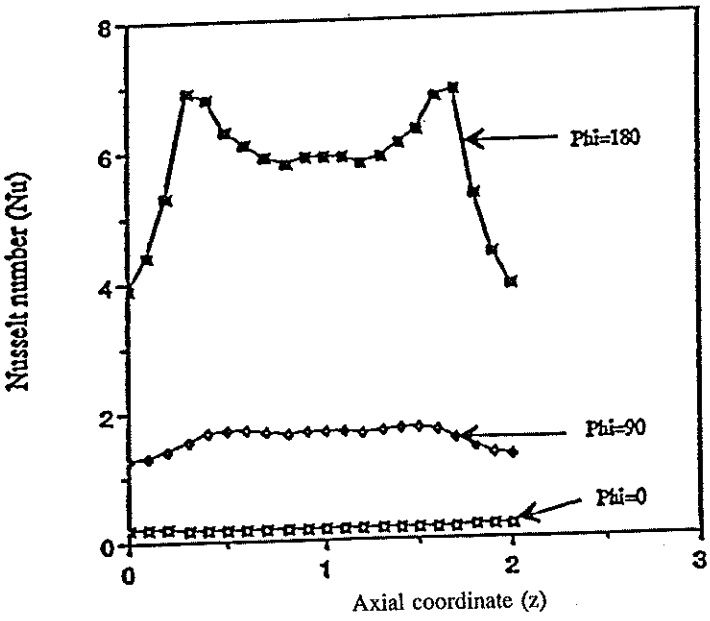

(b)

Fig. 9 Comparison of local Nusselt numbers for outer cylinder (Ra = 10^5, Pr = 5×10^3): (*a*) Takata et al. [12] and (*b*) present work. [Figure 9*a* is reprinted with permission from *International Journal of Heat and Mass Transfer*, vol. 27: Y. Takata, K. Iwashige, K. Fukuda, and S. Hasegawa, Three-Dimensional Natural Convection in an Inclined Cylindrical Annulus, copyright © 1984, Pergamon Press Ltd.]

ence between the Nusselt numbers in the two cases was found to be within 2.5%. It should be noted that the FDM results obtained by Vafai and Ettefagh [22] were in one-to-one agreement with those of Takata et al. [12].

Case 3: Comparison of Results for Three-Dimensional Open Ended Annuli

Numerical simulation of the convective energy transfer process in an open annulus is carried out by making use of an extended computational domain at the end. This procedure is required for implementing the virtually unknown boundary conditions at the open end. A sketch of the computational domain for an open-ended annulus of length $2L_1$ is shown in Fig. 10. The boundary conditions for this problem are as follows:

Curved surface (1) of the inner cylinder

$$u_x = u_y = u_z = 0 \qquad T = T_1 \qquad \text{at } r = \frac{R_1}{R_2} \qquad 0 \le z \le \frac{L}{R_2} \tag{19}$$

Curved surface (2) of the outer cylinder

$$u_x = u_y = u_z = 0 \qquad T = T_2 \qquad \text{at } r = 1 \qquad 0 \le z \le \frac{L}{R_2} \tag{20}$$

Vertical (flat) surface (3) of the inner cylinder

$$u_x = u_y = u_z = 0 \qquad \frac{\partial T}{\partial z} = 0 \qquad \text{at } z = \frac{L}{R_2} \qquad 0 \le r \le \frac{R_1}{R_2} \tag{21}$$

Vertical (flat) surface (4) of the outer cylinder

$$u_x = u_y = u_z = 0 \qquad \frac{\partial T}{\partial z} = 0 \qquad \text{at } z = \frac{L}{R_2} \qquad 1 \le r \le \frac{R_e}{R_2} \tag{22}$$

Mid-axial symmetry plane (5)

$$u_z = 0 \qquad \frac{\partial u_x}{\partial z} = \frac{\partial u_y}{\partial z} = \frac{\partial T}{\partial z} = 0 \qquad \text{at } z = 0 \qquad \frac{R_1}{R_2} \le r \le 1 \tag{23}$$

Angular symmetry plane (6)

$$u_y = 0 \qquad \frac{\partial u_x}{\partial y} = \frac{\partial u_z}{\partial y} = \frac{\partial T}{\partial y} = 0 \qquad \frac{R_1}{R_2} \le r \le 1 \tag{24}$$

Numerical simulation of the flow field and heat transfer in open ended structures requires specification of the boundary conditions at the open end. Since it is virtually impossible to impose appropriate boundary conditions at the open end without overconstraining the problem, the simulation should include calculations in an extended compu-

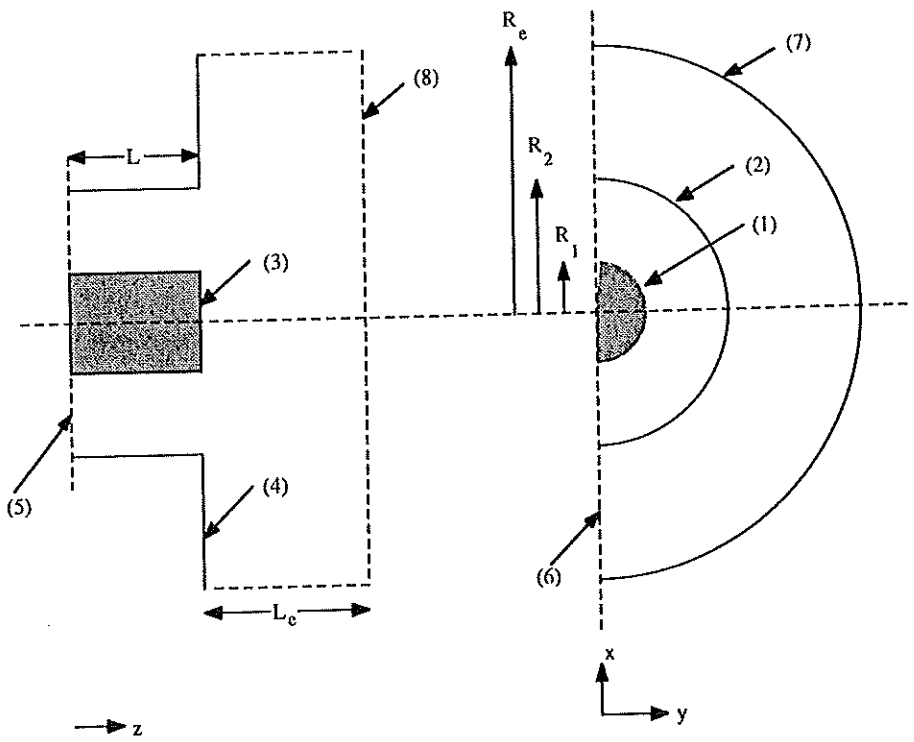

Fig. 10 Physical model and computational domain used for the three-dimensional open ended annulus.

tational domain. This extension not only takes care of the open boundary conditions, but also gives us the opportunity to understand the complex coupling effects between the fluid in the cavity and the ambient surrounding it. In the present study, the extension is a cylinder of radius R_e and length L_e. The choice of these dimensions is made such that further extension will not have a significant effect on the temperature and flow fields inside the annulus and near the opening. These far-field boundary conditions can be stated as follows:

Open radial boundary (7) of the extended computational domain

$$\frac{\partial u_x}{\partial n} = \frac{\partial u_y}{\partial n} = \frac{\partial u_z}{\partial n} = 0 \qquad \frac{\partial T}{\partial n} = 0 \qquad \text{at } r = \frac{R_e}{R_2} \qquad 0 \le z \le \frac{L_e + L}{R_2} \tag{25}$$

Open axial boundary (8) of the extended computational domain

$$\frac{\partial u_x}{\partial z} = \frac{\partial u_y}{\partial z} = \frac{\partial u_z}{\partial z} = 0 \qquad \frac{\partial T}{\partial z} = 0 \qquad \text{at } z = \frac{L_e + L}{R_2} \qquad 0 \le r \le \frac{R_e}{R_2} \tag{26}$$

Studies of buoyancy-induced flows in open ended annuli (case 3) are virtually unknown in the literature. The only concrete work in this field has been carried out by Vafai and Ettefagh [23] and a relevant work was done by Desai and Vafai [25] with respect to

partially open annular cavities in relation to the wheel outboard of an aircraft. Vafai and Ettefagh [23] performed a FDM numerical simulation of natural convection in an open ended annulus bounded by a hot inner cylinder and cold outer cylinder with all plane surfaces of both cylinders insulated. Governing equations were written in a dimensionless vorticity–vector potential form and discretized by using a time-splitting finite-difference algorithm. The annulus considered had a radii ratio of 2.6 and a length to outer cylinder radius ratio of 4. Rayleigh numbers of 4.3×10^3 and 10^4 were considered in their study with air (Pr = 0.7) being the working fluid. Computations were carried out in an extended computational domain. They found that an extension of 3 times the annulus dimensions was necessary to eliminate the far-field effects on the flow field solution inside the cavity for the range of Rayleigh numbers investigated. The boundary conditions used at the ends of the extension to simulate far-field conditions consisted of setting to zero the tangential velocities, the gradients of the temperature, and the normal component of velocity in the normal direction.

The problem studied by Vafai and Ettefagh [23] was solved here using the FEM. Our computations were also carried out in an extended computational domain to take care of the unknown open boundary conditions. The size of the extension for far-field independent results in the case of the finite-element algorithm used here was only twice that of the annulus dimensions. This size of the extended computational domain was determined after extensive numerical experimentation. Thus the solution becomes less dependent on the boundary conditions applied at the far field. Vafai and Ettefagh [23] used a uniform mesh consisting of 70,699 nodes, while our results were obtained with a variable mesh of only 7239 nodes (6016 eight-noded brick elements). Results obtained by the two studies have been compared here for a Rayleigh number of 10^4.

Isotherms at the symmetry plane and the aperture plane using the FDM [23] are shown in Fig. 11. The corresponding isotherms obtained using the FEM solution are also shown. From the figure, it can be easily seen that the results from the two solutions show identical isotherms at the symmetry plane. The clustering of isotherms at the lower portion of the inner cylinder and at the upper portion of the outer cylinder is basically

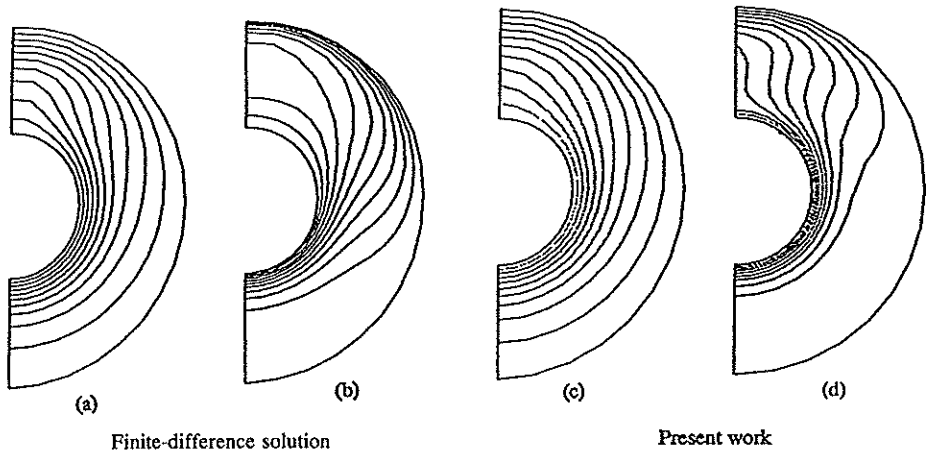

Fig. 11 Comparison of isotherms for an open ended annulus at different axial locations (Ra = 10^4, Pr = 0.7): (*a* and *c*) mid-axial plane and (*b* and *d*) aperture plane. (Figure 11*a* and 11*b* are reprinted from Vafai and Ettefagh [23] with permission from ASME.)

due to the crescent-shaped recirculating pattern in the symmetry plane. Since the length of the annulus is large compared to its radial dimensions, the open boundary effects have not penetrated up to the symmetry plane, and hence the axial component of velocity is almost zero at the symmetry plane. Therefore, the slight distortion of isotherms at the symmetry plane is almost entirely because of the recirculating crescent-shape convective flow in the radial plane. It can be seen that the distortion of isotherms obtained from our solution is significantly greater at the aperture plane. The isotherms are clustered around the entire inner cylinder and at the top of the outer cylinder, indicating the presence of a strong axial flow along these surfaces at the aperture plane. Since the results in the two studies were found to be independent of the mesh size and of extension to the computational domain, the difference in the shape of the isotherms in the two solutions can again be attributed to the inherent limitation of the FEM in capturing some of the details of the flow and temperature fields.

To further bring out the differences between the FDM and FEM solutions, detailed results for the flow field are also presented for Ra = 10^4. Comparisons are once again made quantitatively by making use of the magnitudes of the velocity vectors in the radial planes and qualitatively by means of the contours of axial velocities. Table 4 gives a comparative representation of the FDM and FEM solutions by using the magnitudes of the velocity vectors in the radial plane. From the values shown, it can be seen that the solutions compare well, within 10%.

The axial velocity contours at the aperture plane and also at other radial planes in the annulus are shown in Fig. 12. The contours of the axial velocity obtained from the two cases show a certain degree of discrepancy. Differences in the axial velocity contours become more significant at the aperture plane and at locations close to it, where the open boundary effects are dominant. The finite-element solution (present work) completely misses the penetration of the ambient fluid into the annulus along the top of the inner cylinder surface. Also, the axial velocity component of the outgoing fluid along the bottom surface of the inner cylinder is not captured by our solution. Once again, to verify that the mesh size was not the cause of this discrepancy between the two solutions, an extensive mesh size study was carried out. The number of nodes was increased to 10,698 with a considerable amount of refinement in each of the coordinate directions. But it was observed that the results obtained were essentially independent of the grid size. The mesh refinement could not improve our comparisons. A comparison of the local Nusselt number values over the inner and outer cylinders showed a maximum difference of 18% between the two solutions. This maximum difference is observed at

Table 4 Comparison of Flow Fields for Ra = 10^4 (Open Ended Annulus)

	Maximum value of velocity in the radial plane	
Axial position	FDM	FEM
$L/8$	30.7	32.91
$L/4$	25.1	28.9
$3L/8$	17.8	20.2
L	36.3	40.4

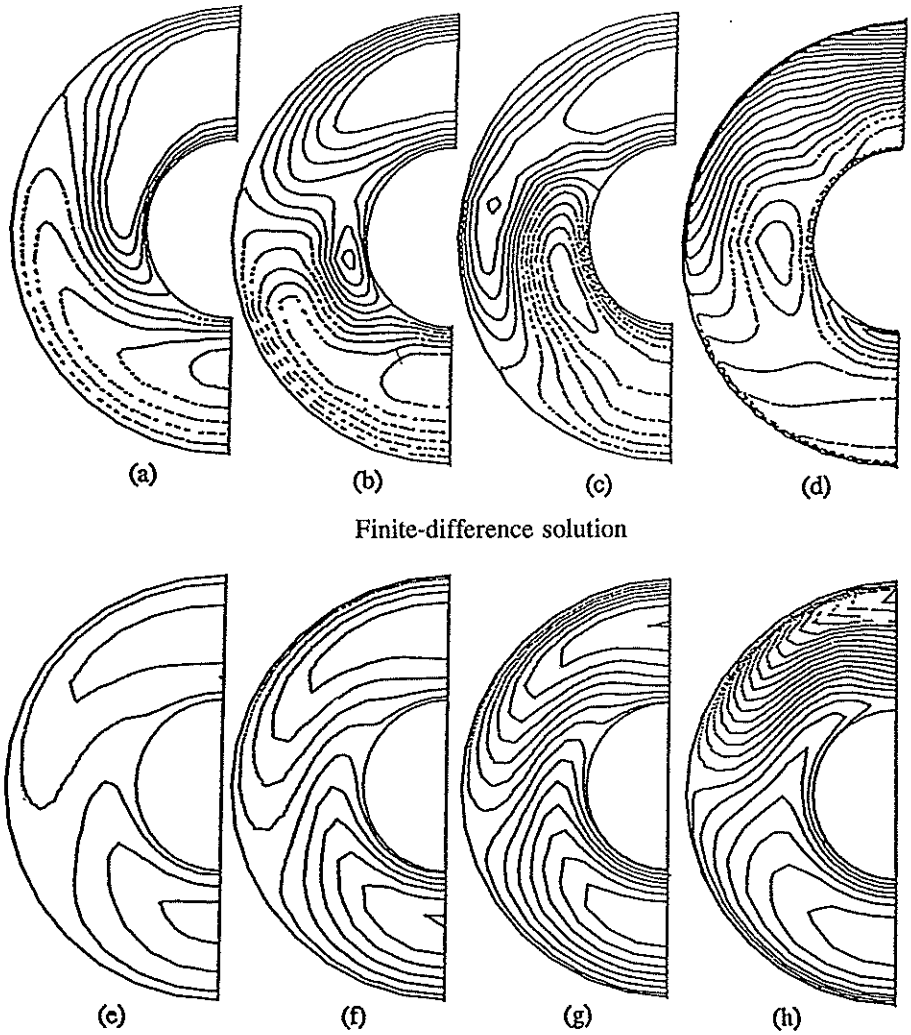

Fig. 12 Comparison of axial velocities for an open ended annulus at different locations (Ra = 10^4, Pr = 0.7): (*a* and *e*) $z = L/8$, (*b* and *f*) $z = L/4$, (*c* and *g*) $z = 3L/8$, and (*d* and *h*) $z = L/2$. (Figure 12*a*, 12*b*, 12*c*, and 12*d* are reprinted from Vafai and Ettefagh [23] with permission from ASME.)

the aperture plane, which is to be expected because of the discrepancy in the flow fields in the two cases.

Again it appears that the FDM is better for obtaining a very accurate solution. The results obtained by the FDM for this case also make more sense physically than those of the FEM solution. The local effects of suction and ejection at the aperture plane, which would cause the fluid to come in and go out of the cavity through small areas around the inner cylinder, are not captured by the finite-element scheme. However, the overall physics of the problem is captured quite well by the finite-element solution.

CONCLUSIONS

A comparative analysis of the finite-element and finite-difference methods for buoyancy-driven flows in closed and annular cavities has been presented. Based on the results presented here, it can be concluded that the FEM gives solutions of the same accuracy for the two-dimensional model with much coarser grid structure than that used for the FDM solution. For the three-dimensional closed annulus, at low Rayleigh numbers, the solutions obtained by the two techniques are almost the same. Once again, significant savings in CPU time can be achieved through the use of a coarse grid structure with the FEM. However, at higher Rayleigh numbers, the flow becomes more complicated, and the solution obtained by the FEM deteriorates. The results presented here show the inherent differences between the two techniques. As is demonstrated by the results presented here, the FEM gives solutions that are fairly accurate and with significantly reduced CPU time. Hence, for most practical problems, the flow and temperature fields can be predicted more efficiently and economically by the FEM. If the minute details of the variable field are required, the FDM is the preferred method of solution. Comparison of the solutions for the open ended annulus further emphasizes our recommendations.

REFERENCES

1. T. H. Kuehn and R. J. Goldstein, An Experimental and Theoretical Study of Natural Convection in the Annulus between Horizontal Concentric Cylinders. *J. Fluid Mech.*, vol. 74, pp. 695–719, 1976.
2. Y. T. Tsui and B. Tremblay, On Transient Natural Convection Heat Transfer in the Annulus between Concentric, Horizontal Cylinders with Isothermal Surfaces, *Int. J. Heat Mass Transfer*, vol. 27, pp. 103–111, 1984.
3. R. E. Powe, C. T. Carley, and S. L. Carruth, A Numerical Solution for Natural Convection in Cylindrical Annuli. *ASME J. Heat Transfer*, vol. 92, pp. 210–220, 1971.
4. A. Aziz and J. D. Hellums, Numerical Solutions of the Three-Dimensional Equations of Motion for Laminar Natural Convection, *Phys. Fluids*, vol. 10, pp. 314–324, 1976.
5. H. Ozoe, K. Yamamoto, S. W. Churchill, and H. Sayama, Three-Dimensional Numerical Analysis of Laminar Natural Convection in a Confined Fluid Heated from Below, *ASME J. Heat Transfer*, vol. 98C, pp. 202–207, 1976.
6. H. Ozoe, K. Yamamoto, H. Sayama, and S. W. Churchill, Natural Convection Patterns in a Long Inclined Rectangular Box Heated from Below, *Int. J. Heat Mass Transfer*, vol. 20, pp. 131–139, 1977.
7. H. Ozoe, N. Sato, and S. W. Churchill, Experimental Confirmation of the Three-Dimensional Helical Streaklines Previously Computed for Natural Convection in Inclined Rectangular Enclosures, *Int. Chem. Eng.*, vol. 19, pp. 454–462, 1979.
8. R. Viskanta, D. M. Kim, and C. Gau, Three-Dimensional Natural Convection Heat Transfer of a Liquid Metal in a Cavity, *Int. J. Heat Mass Transfer*, vol. 29, pp. 475–485, 1986.
9. D. Kuhn and P. H. Oosthuzien, Three-Dimensional Transient Natural Convective Flow in a Rectangular Enclosure with Localized Heating, Natural Convection in Enclosures, *ASME HTD*, vol. 63, pp. 55–62, 1986.
10. H. Ozoe, T. Okamato, and S. W. Churchill, Natural Convection in a Vertical Annular Space Heated from Below, *Heat Transfer Jpn. Res.*, vol. 8, pp. 82–93, 1979.
11. H. Ozoe, T. Shibata, and S. W. Churchill, Natural Convection in an Inclined Circular Cylin-

drical Annulus Heated and Cooled on Its End Plates, *Int. J. Heat Mass Transfer,* vol. 24, pp. 727–737, 1981.
12. Y. Takata, K. Iwashige, K. Fukuda, and S. Hasegawa, Three-Dimensional Natural Convection in an Inclined Cylindrical Annulus, *Int. J. Heat Mass Transfer,* vol. 27, pp. 747–754, 1984.
13. T. Fusegi and B. Farouk, A Three-Dimensional Study of Natural Convection in an Inclined Cylindrical Annulus, *Heat Transfer 1986: Proc. Eighth Heat Transfer Conf., San Francisco, Calif.*, vol. 4, pp. 1575–1580, Hemisphere, Washington, D.C., 1986.
14. Y. Rao, Y. Miki, K. Fukuda, Y. Takata, and S. Hasegawa, Flow Patterns of Natural Convection in Horizontal Concentric Annuli, *Int. J. Heat Mass Transfer,* vol. 28, pp. 705–714, 1985.
15. K. Fukuda, Y. Miki, and S. Hasegawa, Analytical and Experimental Study on Turbulent Natural Convection in a Horizontal Annulus, *Int. J. Heat Mass Transfer,* vol. 33, pp. 629–639, 1990.
16. G. de Vahl Davis and I. P. Jones, Natural Convection in a Square Cavity: A Comparison Exercise, *Int. J. Numer. Meth. Fluids,* vol. 3, pp. 227–248, 1983.
17. H. Ozoe, M. Takemoto, and S. W. Churchill, Finite-Element Analysis of Laminar Natural Convection in Confined Rectangular Regimes—Extrapolation to Zero Element Size, *Numer. Heat Transfer,* vol. 9, pp. 323–333, 1986.
18. C. Taylor and P. Hood, A Numerical Solution of the Navier-Stokes Equations Using the Finite-Element Technique, *Comput. Fluids,* vol. 1, pp. 73–89, 1973.
19. P. M. Gresho, R. L. Lee, and R. L. Sani, On the Time-Dependent Solution of the Incompressible Navier-Stokes Equations in Two and Three Dimensions, in *Recent Advances in Numerical Methods in Fluids,* Pineridge, Swansea, UK, 1980.
20. *FIDAP Theoretical Manual,* Fluid Dynamics International, Evanston, Ill., 1990.
21. M. S. Engelman, G. Strang, and K. J. Bathe, The Application of Quasi-Newton Methods in Fluid Mechanics, *Int. J. Numer. Meth. Eng.*, vol. 17, pp. 707–718, 1981.
22. K. Vafai and J. Ettefagh, An Investigation of Transient Three-Dimensional Natural Convection in a Horizontal Annulus, *Int. J. Heat Mass Transfer,* vol. 34, pp. 2555–2570, 1991.
23. K. Vafai and J. Ettefagh, Axial Transport Effects on Natural Convection Inside of an Open-Ended Annulus, ASME *J. Heat Transfer,* vol. 113, pp. 627–634, 1991.
24. P. L. T. Brian, A Finite-Difference Method of High-Order Accuracy for the Solution of Three-Dimensional Transient Conduction Problems, *AIChE J.*, vol. 7, pp. 367–370, 1961.
25. C. Desai and K. Vafai, Three-Dimensional Buoyancy Induced Flow and Heat Transfer around the Wheel Outboard of an Aircraft, *Int. J. Heat Fluid Flow,* vol. 13, no. 1, pp. 50–64, 1992.

Received 10 May 1991
Accepted 2 October 1991